iScience

CellPress
OPEN ACCESS

Article

Discovering Biomass Structural Determinants Defining the Properties of Plant-Derived Renewable Carbon Fiber

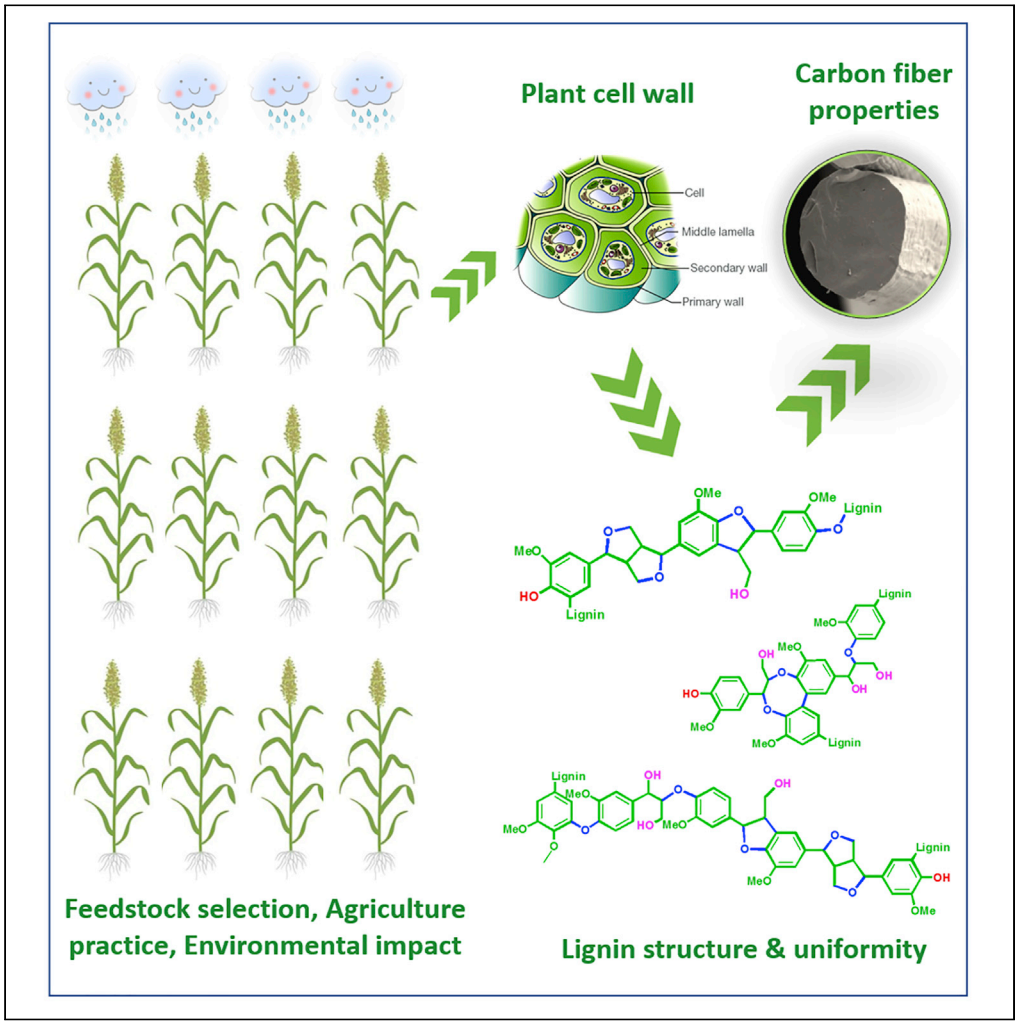

Qiang Li, Cheng Hu, Mengjie Li, ..., Leo Hoffmann, Jr., William L. Rooney, Joshua S. Yuan

syuan@tamu.edu

HIGHLIGHTS

Lignin uniformity was discovered to define biomass-derived CF mechanical property

Traditional key feedstock characteristics do not significantly impact on CF property

Feedstock variants and growth conditions impact on lignin uniformity

Novel feedstock design needs to be developed for biomaterial manufacturing

Li et al., iScience *23*, 101405
August 21, 2020
https://doi.org/10.1016/j.isci.2020.101405

iScience

CellPress
OPEN ACCESS

Article

Discovering Biomass Structural Determinants Defining the Properties of Plant-Derived Renewable Carbon Fiber

Qiang Li,[1] Cheng Hu,[1] Mengjie Li,[1,2] Phuc Truong,[3] Mandar T. Naik,[4] Dwarkanath Prabhu,[1] Leo Hoffmann, Jr.,[5] William L. Rooney,[5] and Joshua S. Yuan[1,6,*]

SUMMARY

Traditional lignocellulosic feedstock research has focused on biomass characteristics essential for improving saccharification efficiency, yet the key biomass features underlying high-quality renewable lignin materials remain unknown. Nevertheless, modern biorefinery cannot achieve sustainability and cost-effectiveness unless the lignin stream can be valorized. We hereby addressed these scientific gaps by investigating biomass characteristics defining lignin-based carbon materials properties. Lignin from eight sorghum samples with diverse characteristics was fabricated into carbon fibers (CFs). Remarkably, only lignin uniformity was found to define CF mechanical performance, highlighting the new structure-property relationship. Contrarily, lignin content and composition did not impact on carbon material properties. Mechanistic study by XRD and Raman spectroscopy revealed that higher lignin uniformity enhanced CF microstructures, in particular, turbostratic carbon content. The study for the first time highlighted lignin uniformity as an important biomass structure determinant for renewable products, which opened up new avenues for feedstock design toward diverse products enabling sustainable and cost-effective bioeconomy.

INTRODUCTION

Lignocellulosic biomass represents the most abundant feedstock for renewable materials. In particular, as the second most abundant biopolymer from plant, lignin has been extensively sought after as a precursor for renewable products and materials (Ragauskas et al., 2014). Traditional research has focused extensively on how biomass characteristics influence its processability for cellulosic ethanol as biofuels (Chen and Dixon, 2007; Mansfield et al., 2012; Studer et al., 2011; Thomas et al., 2017; Van Acker et al., 2014; Yoo et al., 2018) and pulping (Huntley et al., 2003; Lapierre et al., 1999; Pilate et al., 2002; Wagner et al., 2015). However, the recent development revealed that it is essential to derive high-value products out of biomass to enable the biorefinery sustainability and economics. In particular, lignin valorization represents one of the most significant challenges in modern biorefinery (Ragauskas et al., 2014; Tuck et al., 2012). Despite the significance, few researches have focused on how biomass characteristics in feedstock could define the properties of lignin-based carbon materials. In particular, no research has systemically evaluated how different cultivars, lines, and growth environments could impact on lignocellulosic biomass characteristics, which in turn influence the performance of the resultant lignin-based carbon materials.

Despite the imminent needs, the traditional understanding for the impact of biomass characteristics on pretreatment and hydrolysis does not inform the capacity for lignin-based carbon material. In particular, previous studies showed that reducing lignin content improved biomass conversion (Chen and Dixon, 2007; Studer et al., 2011), yet how lignin content, composition, or other characteristics could define the properties of lignin-derived carbon materials is still unknown. There is an urgent need to understand how biomass characteristics impact on the production of lignin-based materials such as carbon fiber (CF), a high-value material with broad applications in the sporting equipment, automotive, wind turbine, and aerospace industries (Li et al., 2017b, 2018a; Titirici et al., 2015). Currently, most carbon fibers are made of a petroleum-derived polyacrylonitrile (PAN) polymer, which accounts for more than half of carbon fiber total cost (Baker and Rials, 2013; Mainka et al., 2015). Lignin as the by-product of the cellulosic

[1]Synthetic and Systems Biology Innovation Hub, Department of Plant Pathology and Microbiology, Department of Chemical Engineering, Texas A&M University, College Station, TX 77843, USA

[2]College of Resources and Environment, Gansu Agricultural University, Lanzhou 730030, China

[3]Soft Matter Facility, Texas A&M University, College Station, TX 77843, USA

[4]Department of Molecular Pharmacology, Physiology and Biotechnology, Brown University, Providence, RI 02903, USA

[5]Department of Soil and Crop Sciences, Texas A&M University, College Station, TX 77843, USA

[6]Lead Contact

*Correspondence: syuan@tamu.edu

https://doi.org/10.1016/j.isci.2020.101405

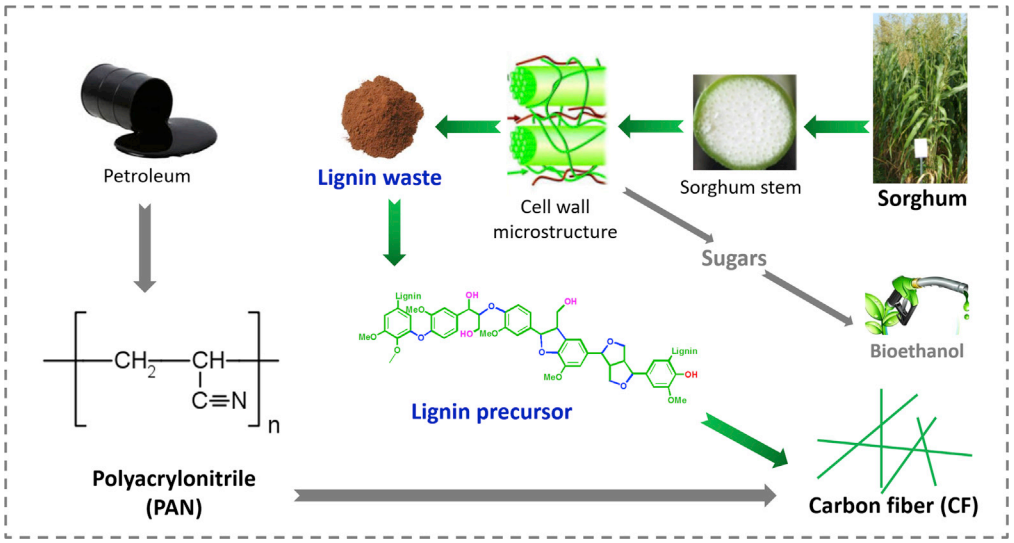

Figure 1. Concept of Valorizing Lignin from Sorghum as an Alternative Precursor of Polyacrylonitrile to Make Carbon Fiber

bioethanol production and pulping mills has high carbon content and plentiful aromatic moieties, representing a promising alternative for PAN for cost-effective carbon fiber production (Figure 1).(Li et al., 2017a) Thereby, the fundamental understanding of the relationship between biomass characteristics and lignin material properties will transform the feedstock development for designing the plant cell wall structure to manufacture quality carbon materials and to enable next-generation integrated biorefinery toward sustainability and cost-effectiveness.

Despite the significance, current research has rendered limited information to guide the design of plant cell wall structure for enhancing the properties of lignin-based carbon materials. On one side, the current research has primarily focused on the optimization of material manufacturing processes and biorefinery designs (Li et al., 2017a, 2017b, 2018a; Jiang et al., 2019), whereas few have studied the impact of feedstock. On the other side, it remains unclear what feedstock characteristics could impact the properties of lignin-based carbon materials. Despite various speculations, the well-defined fundamental understandings on structure-property relationship is crucial in guiding the future feedstock design, which has great potential to promote the development of advanced material manufacturing. Similar concept has been established for engineering lignin biosynthesis to improve cellulosic materials. For example, regulating ferulate 5-hydroxylase (F5H) and caffeic acid *O*-methyltransferase (COMT) has enabled the biosynthesis of hardwood lignin with high content of chemically liable *β*-*O*-4 linkage into a structure similar to softwood lignin (Wagner et al., 2015). Such modification has led to improved cellulosic fiber quality, which concurrently facilitated the delignification in the pulping process and enhanced the fiber quality. Likewise, the chemical features of polymer precursors in biomass feedstocks are likely to define the properties of resultant materials. This fundamental structure-property relationship between lignin chemical characteristics and carbon fiber properties was also evidenced by previous studies of manufacturing processes, where molecular weight, uniformity, linkage profile, and functional group all can potentially impact on carbon fiber properties (Beaucamp et al., 2019; Culebras et al., 2018b; Li et al., 2017a, 2017b, 2018a, 2019b; Zhang et al., 2019). Despite the manufacturing process studies, it is still not clear if these chemical features can be achieved through feedstock improvement and how these chemical features are different in different feedstock cultivars, engineered lines, and growth conditions. Understanding these fundamental questions will help to improve feedstock through breeding, genetic engineering, and growth optimizations to achieve the precursor chemistry for making quality carbon materials from lignocellulosic biomass.

In this study, we have compared the biomass characteristics from different sorghum sessions and identified the chemical features from feedstock defining the carbon fiber properties. The study highlighted that crucial biomass characteristics from traditional studies did not impact carbon material properties. Instead, the study identified new feedstock chemical features essential for carbon fiber properties, paving the path for feedstock improvement to enhance carbon material manufacturing.

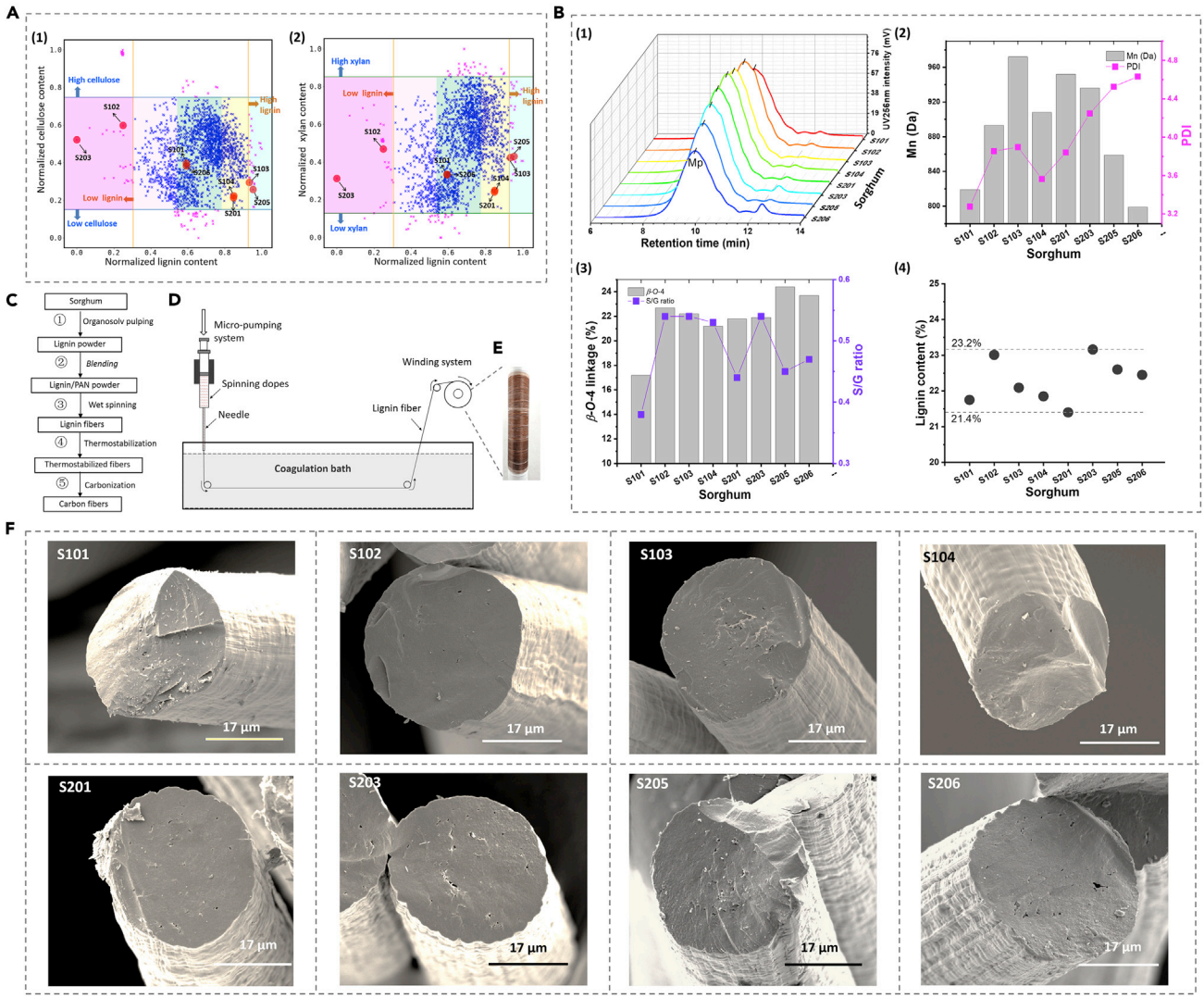

Figure 2. Lignocellulosic Feedstock Selection, Biomass Characteristics of Lignin Features, and the Fabrication of Lignin-based Carbon Fibers

Selection of variant sorghum samples in this research according to lignin content distribution (A), where A-1 and A-2 show the lignin content versus cellulose and xylan, respectively. In (A), the selected eight sorghum samples are highlighted as the magnified red dots, other samples with high or low compositions (cellulose, xylan, and lignin) are magenta dots, whereas most sorghum samples located in the most frequent distribution are blue dots. Moreover, the inserted orange (in A1 and A2), blue (in A1), and green lines (in A2) indicate the thresholds of high and low lignin, cellulose, and xylan distributions, respectively, which are defined as the possibility of the composition distribution as shown in Figure S1 and Table S1. The regions highlighted in magenta, yellow, and cyan are sorghums with moderate cellulose and xylan content but with high, moderate, and low lignin contents, respectively. Chemical characterizations of the extracted sorghum lignin are in (B), where B1–B4 are molecular weight, polydispersity index (PDI), lignin linkage and S/G ratios, and lignin content, respectively. The fabrication process of lignin carbon fiber is in (C), and the (D) displays the wet-spinning setup for lignin fiber formation. (E) and (F) show a representative as-spun precursor fiber roll and the SEM images of the cross sections of the resultant carbon fibers, respectively. All scale bars in (F) are 17 μm.

RESULTS

We hereby aimed to address these fundamental questions by systemically investigating the performance of carbon fibers derived from biomass with diverse characteristics. In particular, we have systemically analyzed molecular weight, polydispersity, content, composition, and linkage profiles of lignin from four different sorghum (*Sorghum bicolor* (L.) Moench) genotypes (R.09072, R.09084, R.09093, R.09098). These four genotypes were selected from 2,067 different sorghum variants according to their biomass compositions as characterized by near-infrared (NIR) spectroscopy (Hoffmann and Rooney, 2014). These sorghum samples were harvested from 60 days after planting in College Station, Texas. As shown in Figure 2A,

sorghum with diverse lignin content distributions but similar cellulose and xylan content distributions was selected. With a focus on lignin, sorghum with high or low cellulose content (Figures 2A1 and S1, Table S1) and high or low xylan content (Figures 2A2 and S1, Table S1) has been excluded. Eight representative sorghum samples were collected from the aforementioned four variants, planting in two different environments (Figure S2). These samples exhibited a wide range of lignin content, including low normalized lignin content (<0.3, sorghum 102 and 203), moderate normalized lignin content (0.5–0.9, sorghum 101, 104, 201, and 206), and high normalized lignin content (>0.9, sorghum 103 and 205) based on NIR analysis (Figures 2A2 and S1, Table S1). The combination of genotypes and growth conditions (as shown in Figure S2) rendered these eight selected sorghum samples with a diverse range of biomass characteristics, which allowed us to build models to best identify the key biomass properties defining renewable carbon fiber performance (Hoffmann and Rooney, 2014). Lignin was extracted by an organosolv pretreatment from these eight sorghum feedstock samples first, and the molecular weight and molecular uniformity (indicated by polydispersity index, PDI) of the extracted lignin were then characterized using size-exclusion chromatography (SEC). As shown in Figures 2B1 and 2B2, lignin molecular weight (Mn) decreased in the order: sorghum 103 > sorghum 201 > sorghum 203 > sorghum 104 > sorghum 102 > sorghum 205 > sorghum 101 > sorghum 206, whereas lignin molecular uniformity decreased in the order: sorghum 101 > sorghum 104 > sorghum 102 > sorghum 201 > sorghum 103 > sorghum 203 > sorghum 205 > sorghum 206 (smaller PDI means higher uniformity). In addition, the interunitary linkages and composition of lignin from these eight sorghum feedstock were analyzed using 2D HSQC NMR and the linkage profiles of uncondensed β-*O*-4, condensed β-5, and condensed β-β were calculated based on 100 aromatic rings of syringyl (S), guaiacyl (G), and ρ-hydroxyphenyl (H) units (see the assignments of the linkages and units in Table S2). The frequencies of β-*O*-4, β-5, and β-β linkages were 17.2%–24.4%, 10.1%–11.8%, and 2.2%–4.2%, respectively (Figures 2B3 and S3). The S/G ratio of lignin ranged from 0.385 (sorghum 101) to 0.542 (sorghum 102 and 203) (Figures 2B3 and S4). In terms of lignin content, these sorghum feedstocks ranged from 21.2% (sorghum 203) to 23.0% (sorghum 102) (Figure 2B4 and Table S3). Considering the diverse range of lignin characteristics, lignin from these eight sorghum feedstock samples could serve as perfect model precursors to elucidate how biomass characteristics will impact on the performance of the resultant carbon fibers. Such study will open up the path to select plant cultivar, design biomass feedstock, and define growth conditions to derive cell wall structures for manufacturing high-quality carbon fiber.

Lignin-based carbon fiber was manufactured using a customized wet-spinning facility as shown in Figure 2D. Wet spinning has been widely used in carbon fiber industry and is feasible for all types of lignin, especially the infusible lignin with more condensed structures. These types of lignin would require structural modification to enable melt spinning (Culebras et al., 2018a). To prepare spinning dopes, lignin powders were mixed with PAN polymers (50%:50%, w/w) and dissolved in *N*,*N*-dimethylformamide (DMF) (Figure 2C). With current technologies, the replacement of lignin at higher percentage (more than half) significantly decreased the spinnability of the dopes, resulting in non-continuous spinning and uneven fibers. Since more than 50% of total cost of the PAN-based carbon fiber lies in its PAN precursor (Baker and Rials, 2013), a replacement of 50% of PAN by the waste lignin polymer could significantly reduce the cost of traditional carbon fiber industry, while achieving acceptable properties for broad applications. The as-spun precursor fibers, as shown in Figure 2E, were then thermostabilized at 250°C and carbonized at 1,000°C to prepare carbon fibers (Figure 2C). Scanning electron microscopy (SEM) analysis revealed the morphologies and structures of the resultant lignin-based carbon fibers along the fibers and on the fiber cross sections. As shown in Figures 2F and S6, all carbon fibers displayed flat-layer-like transverse textures similar to commercial pitch-based carbon fibers (Singer, 1981; Edie, 1998), although several defects of irregular debris and pores were found on carbon fiber cross sections. These porous structures have been significantly reduced by process optimization, including carefully degassing of spinning dopes by sonication, well controlling wet spinning process, and carefully controlling the coagulation bath temperature and concentration. The mechanical performance of a single carbon fiber was subsequently measured to determine the relationship between different biomass characteristics and carbon fiber performances (see a typical stress-strain curve in Figure S7).

Surprisingly, significant differences were found in the mechanical performances of the resultant carbon fiber, in terms of tensile strength, modulus of elastics (MOE), and elongation (Figures 3A–3C). For the carbon fibers made of lignin from sorghum 101, 104, and 201, the tensile strength varied from 339 to 380 MPa, MOE was 32.6–37.8 GPa, and the elongation was 1.18%–1.20%. These data were higher than that of sorghum 102 and 103, for which the tensile strength was 283 and 272 MPa, MOE was 30.4 and 30.0 GPa, and elongation was 1.06% and 1.05%, respectively. The mechanical properties of all aforementioned carbon fibers were

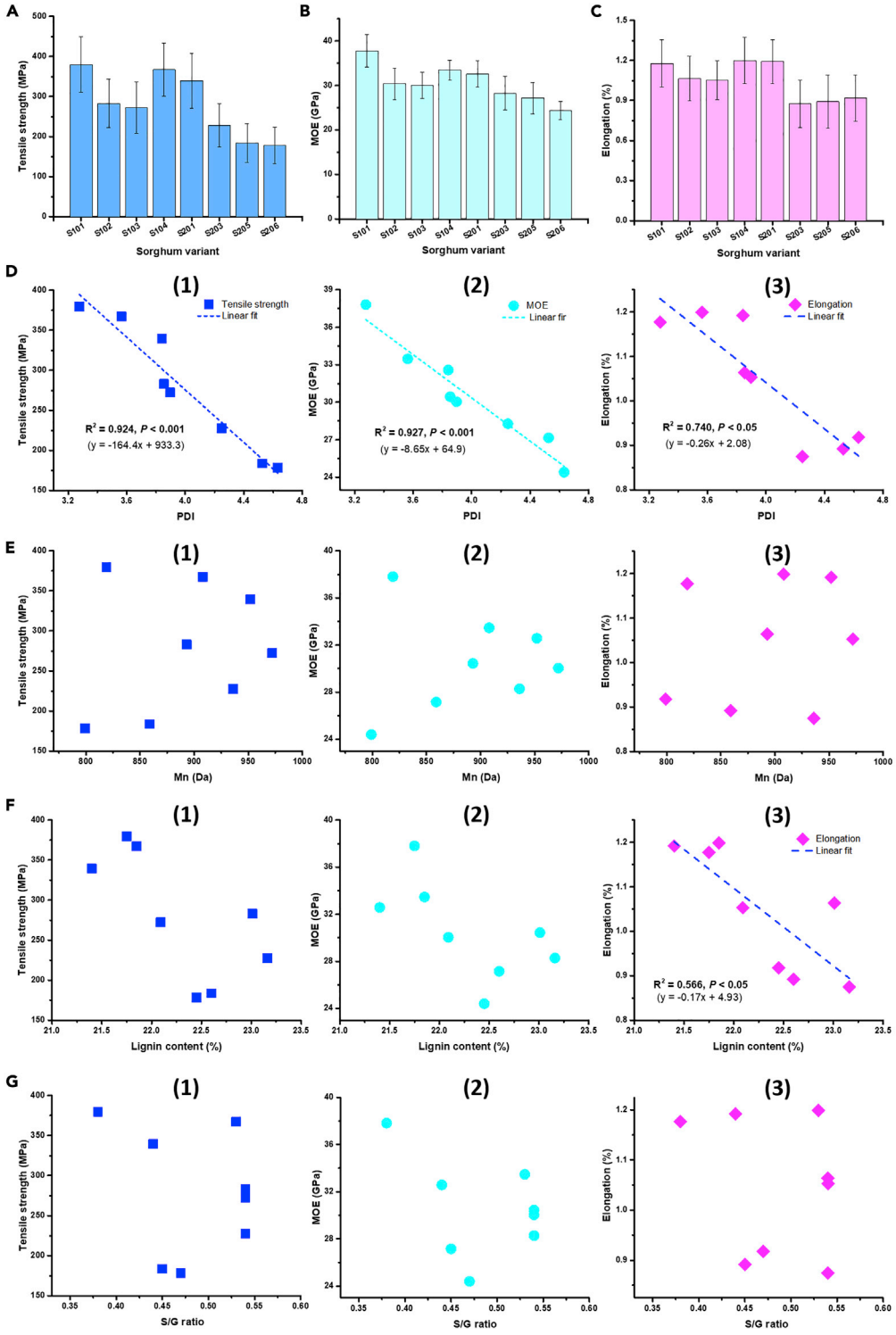

Figure 3. The Mechanical Properties of Lignin-based Carbon Fibers and their Correlation Relationships with Biomass Characteristics

The mechanical performances of tensile strength (A), modulus of elasticity (MOE, B) and elongation (C) of carbon fibers made of lignin derived from eight sorghum samples with diverse biomass characteristics. Scatterplots show the

relationships between each mechanical performance and lignin molecular uniformity (PDI), molecular weight, lignin content, and S/G ratio, as displayed in (D)–(G), respectively. PDI, Mn, lignin content, and S/G ratio are shown as a function of tensile strength (1), MOE (2), and elongation (3), respectively. The error bars in (A)–(C) are calculated based on 25 different carbon fibers.

better than the third group of sorghum 203, 205, and 206, for which the tensile strength was 178–228 MPa, MOE was 24.4–28.3 GPa, and elongation was 0.88%–0.92%, respectively. The results were out of expectation, in that the lignin derived from the same sorghum species could be used to manufacture carbon fibers with significantly different performance (comparing sorghum 101 and 206, sorghum 102 and 203, sorghum 103 and 205, and sorghum 104 and 201). Therefore, feedstock selection, development, and growth condition should be important considerations for manufacturing quality materials from biomass. The impact of feedstock characteristics on carbon fiber performance has not been considered in previous studies. More importantly, the results highlighted the essential fundamental questions regarding how biomass characteristics could impact the properties of the lignin-derived materials.

In order to decipher the fundamental relationship between biomass characteristics and carbon fiber properties, we carried out comprehensive linear regression analysis of various lignin features versus carbon fiber performances to elucidate the underlying mechanisms controlling carbon fiber quality. The key features of biomass characteristics including lignin content, composition (S/G ratio), molecular weight, and molecular uniformity were used as independent variables to perform the linear regression with carbon fiber tensile strength, MOE, and elongation as dependent variables, respectively (Figures 3D–3G). Even though lignin content has been previously shown to define the saccharification efficiency and ethanol yield (Chen and Dixon, 2007), we found that lignin content was not correlated to carbon fiber tensile strength and MOE (Figures 3F1 and 3F2). This is in contrast to the original hypothesis that lignin content and composition could play an important role in the properties of renewable carbon fiber. Although lignin content had correlation with elongation weakly ($P < 0.05$), the correlation determinations (R^2) was as low as 0.566 (Figure 3F3). These data indicated that lignin content might not significantly impact on the carbon fiber performance as it does for biomass conversion. More interestingly, neither lignin composition (Figure 3G) nor molecular weight (Figure 3E) impacted on the carbon fiber mechanical performance, too. Nevertheless, significant correlations were found between lignin molecular uniformity and carbon fiber mechanical performance. As shown in Figure 2B2, sorghum 101, 104, and 201 (PDI 3.28–3.84) had lower PDI than both sorghum 102 (3.85) and 103 (3.90) and had much lower PDI than sorghum 203, 205, and 206 (4.25–4.63), suggesting more uniform lignin polymers (smaller PDI) in these sorghum samples. These sorghum samples (101, 104, and 201) all had much improved mechanical performances of the lignin-based carbon fibers (Figures 3A–3C). In fact, linear regression analysis showed strong negative correlations between lignin PDI and carbon fiber mechanical performances. As shown in Figure 3D, we found linear correlations between PDI and tensile strength ($R^2 = 0.924$, $P < 0.001$), MOE ($R^2 = 0.927$, $P < 0.001$), and elongation ($R^2 = 0.740$, $P < 0.05$). The results thus highlighted that biomass characteristics have an impact on the mechanical performance of the resultant carbon fiber. Unlike the processability of lignocellulosic biomass impacted by the lignin content and S/G ratio (Chen and Dixon, 2007; Studer et al., 2011; Wagner et al., 2015), the results highlighted that more uniform lignin in feedstock could significantly enhance the mechanical performances of the resultant lignin-based carbon fibers. Overall, the results highlighted three aspects of finding: (1) biomass characteristics impact lignin-derived carbon fiber performance; (2) lignin uniformity, instead of molecular weight, content, and composition, defines the carbon fiber properties; (3) there are huge variations in lignin molecular uniformity even within the same feedstock species.

The performances of carbon fibers are directly related to their crystallite microstructure, in particular, the content and size of pre-graphitic turbostratic carbon (Frank et al., 2014; Li et al., 2017b). Such microstructure comprised more- or less-bent crystallite layers with sp^2-hybridized carbon atoms in carbon fiber (Frank et al., 2014). In order to understand the fundamental mechanisms of how lignin characteristics in sorghum biomass define carbon fiber performances, the microstructures of the resultant lignin-based carbon fibers were analyzed using both XRD and Raman spectroscopy. First, the crystallite size (L_{hkl}) and the distances between interfacial crystallite layers (d_{hkl}) were calculated from XRD diffractograms (Figure S8) using Scherrer's equation and Bragg's law, respectively. As shown in Figures 4A1 and 4A2, L_{hkl} varied from 1.016 nm (sorghum 205) to 1.252 nm (sorghum 101) and the d_{hkl} was in the range of 0.366 nm (sorghum 206) to 0.356 nm (sorghum 101). Second, the ratios of the graphite (G) band and

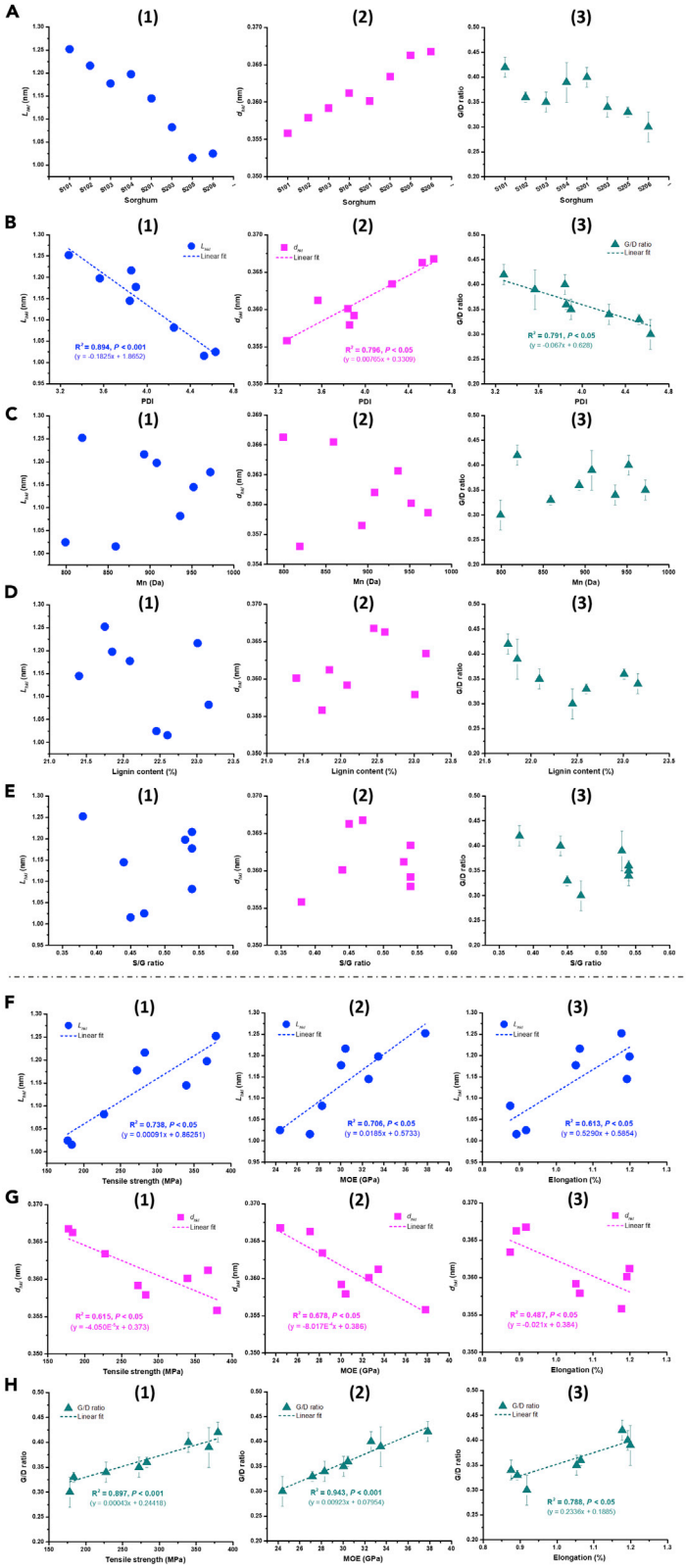
A
(1)
(2)
(3)
Sorghum
B
(1)
(2)
(3)
PDI
C
(1)
(2)
(3)
Mn (Da)
D
(1)
(2)
(3)
Lignin content (%)
E
(1)
(2)
(3)
S/G ratio
F
(1)
(2)
(3)
Tensile strength (MPa)
MOE (GPa)
Elongation (%)
G
(1)
(2)
(3)
Tensile strength (MPa)
MOE (GPa)
Elongation (%)
H
(1)
(2)
(3)
Tensile strength (MPa)
MOE (GPa)
Elongation (%)

Figure 4. Microstructures in Lignin Carbon Fiber and Their Relationships with Lignin Molecular Uniformity, Molecular Weight, Content, and S/G Ratio as well as the Mechanical Performance of the Resultant Carbon Fibers

A1 and A2 in (A), L_{hkl} and d_{hkl} calculated from XRD; A3, G/D ratio measured by Raman spectroscopy. (B)–(E) Relationship between microstructures (L_{hkl}, d_{hkl}, and G/D ratio) and PDI, Mn, lignin content, and S/G ratio, respectively. (F)–(H) Relationship between L_{hkl}, d_{hkl}, and G/D ratio and mechanical performances (tensile strength, MOE, and elongation), respectively. Blue circles, L_{hkl}; magenta squares, d_{hkl}; dark cyan triangles, G/D ratio. The error bars are calculated from three trials.

disordered (D) band (G/D ratios) in carbon fibers were characterized by Raman spectroscopy (Figure S9), which had the highest value of 0.42 for sorghum 101 and the lowest value of 0.30 for sorghum 206 (Figure 4A3). All these data of carbon fiber microstructures were then fitted with PDI, molecular weight, lignin content, and S/G ratios into linear regression to define their relationships. Significant correlations between the microstructures (L_{hkl}, d_{hkl} and G/D ratio) and PDI were discovered (Figures 4B1–B3). However, these microstructure characteristics did not correlate with the molecular weight (Figure 4C), lignin content (Figure 4D), or lignin S/G ratio (Figure 4E). The results were consistent with the correlations between mechanical performances and lignin features as displayed in Figures 3D–3G. Thus, the molecular uniformity of lignin polymer in sorghum defined the microstructures and the carbon fiber mechanical performances, whereas biomass characteristics such as lignin molecular weight, lignin content, and S/G ratio may not be main factors affecting the microstructures and the mechanical performance of the carbon fibers.

To further determine the impacts of each microstructure characteristics such as L_{hkl}, d_{hkl}, and G/D ratio on the mechanic performances of lignin-based carbon fibers, linear regressions were fitted for tensile strength, MOE, and elongation against these characteristics. In fact, all microstructure characteristics of L_{hkl}, d_{hkl}, and G/D ratio had significant linear correlations with mechanical performance properties (Figures 4F–4H), indicating that crystallite size (L_{hkl}), crystallite content (G/D ratio), and the distances between crystallite layers (d_{hkl}) all impact on the carbon fiber performances. Moreover, when these correlation relationships were compared, the correlation determinations (R^2) of G/D ratio versus tensile strength (R^2 = 0.897), MOE (R^2 = 0.943), and elongation (R^2 = 0.788) were much larger than those of both L_{hkl} versus tensile strength (R^2 = 0.738), MOE (R^2 = 0.706), and elongation (R^2 = 0.613) and d_{hkl} versus tensile strength (R^2 = 0.615), MOE (R^2 = 0.678), and elongation (R^2 = 0.487), respectively. Therefore, as compared with the crystallite size and the distance between crystallite layers, the crystallite content may be a stronger determinant for the properties of lignin-based carbon fibers. The lignin characteristics enabling more microstructures with larger size and smaller distance between crystallite layers thus would help to further enhance the mechanical performance of current lignin-based carbon fibers.

DISCUSSION

Overall, we hereby identified a largely overlooked biomass characteristics, lignin molecular uniformity, as the key determinant for the mechanical properties of biomass-derived carbon fiber. The underlying mechanisms indicated that more uniform lignin from biomass feedstock will improve carbon fiber microstructures, particularly, the content of crystallite in carbon fibers along with the size and inter-layer distance. The identification of lignin uniformity as a key biomass characteristic represents a completely new perspective, as traditional biomass research has been focused on tailoring lignin content and composition toward improved saccharification efficiency. Nevertheless, considering that it is essential to develop high-value products like carbon fiber from biomass, such new perspective will have profound impact on renewable energy and materials. First, from feedstock development and plant biology perspective, extensive efforts have been put into studying the molecular and biochemical mechanisms regulating plant lignin biosynthesis to achieve optimal content and composition during the past decades (Chen and Dixon, 2007; Huntley et al., 2003; Li et al., 2008; Pilate et al., 2002; Wagner et al., 2015). These researches have significantly advanced our understanding on monolignol biosynthesis and developed various feedstock with improved biomass conversion. However, the field largely ignored the scientific questions underlying the development of high-value products, although high-value products could be essential for biorefinery sustainability and cost-effectiveness (Mohanty et al., 2018; Ragauskas et al., 2014; Tuck et al., 2012). Unlike lignin content and composition determined largely by monolignol biosynthesis, lignin uniformity within feedstock could be controlled by more complicated factors that are still much less understood by the scientific community. It is speculated that the monomer type could impact lignin structural uniformity, since the polymerization patterns could be reformed by manipulating monolignols. For example, lignin derived from caffeoyl

alcohol has been proved to possess a uniform benzodioxane structure (Li et al., 2018b). Recent studies indicated that extracellular plant laccase could involve in lignin polymerization (Zhao et al., 2013), yet their roles in controlling lignin uniformity are still unknown. We therefore need to explore what enzymes and regulators determine the lignin uniformity, which is a very new direction for plant biology and feedstock development.

Second, from lignocellulosic biorefinery perspective, biorefinery might not achieve economic feasibility and overall sustainability unless various value-added products are developed (Maity, 2015; Tuck et al., 2012). Lignin products, in particular, carbon materials, have been explored as key options to address the biorefinery challenges (Ragauskas et al., 2014; Tuck et al., 2012; Wang et al., 2019). Previously, research also highlighted that lignin uniformity could be changed during biomass deconstruction and lignin processing (Chatterjee and Saito, 2015; Laurichesse and Avérous, 2014). Our recent advancements in lignin fractionation have shown the potential to improve lignin molecular uniformity by new biorefinery procedures (Li et al., 2017a, 2017b, 2018a). Additionally, lignin out of different processing generally has variant functional groups and molecular weight, all of which altered the thermal behavior of the resultant lignin fiber (Culebras et al., 2018b). Traditional biorefinery configurations thus need to be tailored to produce a lignin stream with better uniformity, if high-value carbon materials like carbon fiber needs to be produced as value-added products. Eventually, the new feedstock development and process design strategies will together provide a holistic approach to improve lignin uniformity and control polymer chemistry for manufacturing high-value materials from biorefinery waste.

Third, from the renewable materials perspective, the new finding opened up the new avenues to use lignin by-products from both pulping and paper industry and biorefinery to produce high-value carbon materials. It is possible that feedstock with new cell wall structure could be developed to enable such by-product utilization. Fractionation and other processing technologies could also be developed to deliver more uniform lignin for versatile carbon materials (Culebras et al., 2019; Dalton et al., 2019; Li et al., 2019a). The fundamental understanding of the underlying relationship between lignin structure and carbon fiber property will allow the new renewable material design from biomass and other biological sources.

Fourth, from the agricultural practice perspective, the research also has significant implications. As shown in Figure S2, sorghum lignin uniformity is heavily impacted by the growth location. Likewise, other crop and bioenergy feedstocks could have similar differential biomass characteristics. For example, natural poplar variants (Meng et al., 2017) and engineered switchgrass (Liu et al., 2018) had significant differences in lignin uniformity. It is critical to identify the impacts of environmental factors like soil nutrition, water content, rainfall, and temperature and agricultural practices like tillage, fertilization, and harvesting on biomass characteristics, so that a stable supply chain can be established to manufacture quality carbon fiber from biomass. Moreover, producing high-value materials like carbon fiber using agricultural residues and biorefinery waste could significantly improve the economic return, reduce the CO_2 footprint, promote rural economy, and provide sustainable solutions for emerging societal challenges in environment and energy, all of which could profoundly transform the bioeconomy.

In summary, the molecular uniformity of lignin polymer in sorghum was revealed as a critical determinant defining the quality of the resultant lignin-based carbon fibers. The study indicated that further research to design feedstock, improve agricultural practice, control environmental factors, and reconfigure biomass processing will be needed to manufacture value-added lignin materials from lignocellulosic biorefinery (Figure 5). The mechanistical studies on how feedstock designing can change the polymer structure of plant cell wall components (feedstock-structure relationship) and how the changed polymer structure can advance both lignocellulosic biorefinery and biomaterial manufacturing (structure-property relationship) are still quite open. The finding of lignin uniformity formed in the cell walls of sorghum variants and its determination on lignin carbon fiber performance can also inform the regulation of other plant cell wall polymers like cellulose and hemicellulose toward their functional applications (Figure 5). All these future advancements could open a novel avenue to transform the whole bioeconomy.

Limitations of the Study

We revealed lignin uniformity as the key biomass structural characteristic defining the pre-graphitic turbostratic carbon structure and mechanical performances of sorghum-derived lignin-based carbon fibers. The

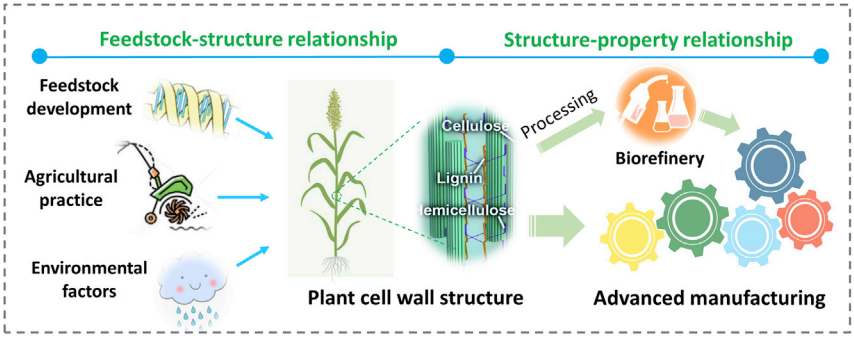

Figure 5. Illustration of a New Avenue to Transform Current Lignocellulosic Biorefinery and Advanced Manufacturing by Regulating Polymer Structures of Plant Cell Wall Components

Feedstock-structure relationship is to reveal how feedstock developments, agricultural practices, and environment factors could regulate polymer structure and enable plant cell wall design; structure-property relationship can inform the reconfiguration of biomass processing for integrated biorefinery and advanced manufacturing for bioeconomy. These future advancements for the research field can expand from lignin uniformity as highlighted in this research to other novel lignin characteristics as well as other plant cell polymers like cellulose and hemicellulose.

study might need more evidences such as different biomass to further prove the discovery. Mechanistic understanding of how lignin uniformity is controlled in biomass still awaits elucidation, representing another limitation of the study. Current mechanical performances of our carbon fibers are still low. Their further improvements by integrating other technologies (such as graphitization and post treatment) are needed to make these renewable carbon fibers implementable in industry.

Resource Availability

Lead Contact

Further information and requests for lignocellulosic resources and carbon materials should be directed to and will be fulfilled by the Lead Contact, Joshua S. Yuan (syuan@tamu.edu).

Materials Availability

The lignin samples extracted from sorghum variants and the generated carbon fibers are available from the corresponding author. The raw sorghum feedstocks are available from the corresponding author upon reasonable request.

Data and Code Availability

All data presented in this study are available from the corresponding author upon reasonable request.

METHODS

All methods can be found in the accompanying Transparent Methods supplemental file.

SUPPLEMENTAL INFORMATION

Supplemental Information can be found online at https://doi.org/10.1016/j.isci.2020.101405.

ACKNOWLEDGMENTS

The authors would like to thank Dr. Anup K. Bandyopadhyay in Department of Materials Science and Engineering (MSEN), Texas A&M University for his assistance of XRD characterizations and Dr. Thomas C. Stephens in Microscopy Image Center (MIC), Texas A&M University for his assistance with SEM. The authors also acknowledge the funding supports of Texas A&M Energy Institute Seed Grant to J.S.Y., Texas A&M University T3 grant to J.S.Y. and W.L.R., and DOE EERE BETO grants (DE-EE0007104, DE-EE0006112, and DE-EE0008250) to J.S.Y. The authors also acknowledge Alicat Scientific, Inc. for contributing flow meters system for the carbon fiber manufacturing system.

AUTHOR CONTRIBUTIONS

Q.L. and J.S.Y. designed the experiments. Q.L., C.H., and M.L. carried out lignin extraction and fiber spinning. Q.L. did lignin characterizations using SEC with P.T. and 2D HSQC with M.T.N. L.H. Jr. and W.L.R. provided sorghum feedstock and all NIR data. D.P. assisted Q.L. with analysis of NIR data for sorghum selection. Q.L. did all carbon fiber characterizations. Q.L. wrote the manuscript and J.S.Y. revised it. J.S.Y. supervised the research. All authors contributed to the scientific discussions and comments on the manuscript.

DECLARATION OF INTEREST

The authors declare no competing interests.

Received: December 26, 2019
Revised: June 3, 2020
Accepted: July 21, 2020
Published: August 21, 2020

REFERENCES

Baker, D.A., and Rials, T.G. (2013). Recent advances in low-cost carbon fiber manufacture from lignin. J. Appl. Polym. Sci. *130*, 713–728.

Beaucamp, A., Wang, Y., Culebras, M., and Collins, M.N. (2019). Carbon fibres from renewable resources: the role of the lignin molecular structure in its blendability with biobased poly(ethylene terephthalate). Green. Chem. *21*, 5063–5072.

Chatterjee, S., and Saito, T. (2015). Lignin-derived advanced carbon materials. ChemSusChem *8*, 3941–3958.

Chen, F., and Dixon, R.A. (2007). Lignin modification improves fermentable sugar yields for biofuel production. Nat. Biotechnol. *25*, 759–761.

Culebras, M., Beaucamp, A., Wang, Y., Clauss, M.M., Frank, E., and Collins, M.N. (2018a). Biobased structurally compatible polymer blends based on lignin and thermoplastic elastomer polyurethane as carbon fiber precursors. ACS Sustainable Chem. Eng. *6*, 8816–8825.

Culebras, M., Geaney, H., Beaucamp, A., Upadhyaya, P., Dalton, E., Ryan, K.M., and Collins, M.N. (2019). Bio-derived carbon nanofibres from lignin as high-performance Li-ion anode materials. ChemSusChem *12*, 4516–4521.

Culebras, M., Sanchis, M.J., Beaucamp, A., Carsí, M., Kandola, B.K., Horrocks, A.R., Panzetti, G., Birkinshaw, C., and Collins, M.N. (2018b). Understanding the thermal and dielectric response of organosolv and modified kraft lignin as a carbon fibre precursor. Green. Chem. *20*, 4461–4472.

Dalton, N., Lynch, R.P., Collins, M.N., and Culebras, M. (2019). Thermoelectric properties of electrospun carbon nanofibres derived from lignin. Int. J. Biol. Macromol. *121*, 472–479.

Edie, D.D. (1998). The effect of processing on the structure and properties of carbon fibers. Carbon *36*, 345–362.

Frank, E., Steudle, L.M., Ingildeev, D., Sporl, J.M., and Buchmeiser, M.R. (2014). Carbon fibers: precursor systems, processing, structure, and properties. Angew. Chem. Int. Ed. Engl. *53*, 5262–5298.

Hoffmann, L., Jr., and Rooney, W.L. (2014). Accumulation of biomass and compositional change over the growth season for six photoperiod sorghum lines. Bioenergy Res. *7*, 811–815.

Huntley, S.K., Ellis, D., Gilbert, M., Chapple, C., and Mansfield, S.D. (2003). Significant increases in pulping efficiency in C4H-F5H-transformed poplars: improved chemical savings and reduced environmental toxins. J. Agric. Food Chem. *51*, 6178–6183.

Jiang, P., Li, Q., Gao, C., Lu, J., Cheng, Y., Zhai, S., An, Q., and Wang, H. (2019). Fractionation of alkali lignin by organic solvents for biodegradable microsphere through self-assembly. Bioresour. Technol *289*, 121640–121647.

Lapierre, C., Pollet, B., Petit-Conil, M., Toval, G., Romero, J., Pilate, G., Leplé, J.-C., Boerjan, W., Ferret, V., De Nadai, V., and Jouanin, L. (1999). Structural alterations of lignins in transgenic poplars with depressed cinnamyl alcohol dehydrogenase or caffeic acid *O-Methyltransferase* activity have an opposite impact on the efficiency of industrial kraft pulping. Plant Physiol. *119*, 153–164.

Laurichesse, S., and Avérous, L. (2014). Chemical modification of lignins: towards biobased polymers. Prog. Polym. Sci. *39*, 1266–1290.

Li, Q., Hu, C., Clarke, H., Li, M., Shamberger, P., Wu, W., and Yuan, J.S. (2019a). Microstructure defines the electroconductive and mechanical performance of plant-derived renewable carbon fiber. Chem. Comm. *55*, 12655–12658.

Li, Q., Li, M., Lin, H.-S., Hu, C., Truong, P., Zhang, T., Sue, H.-J., Pu, Y., Ragauskas, A.J., and Yuan, J.S. (2019b). Non-solvent fractionation of lignin enhances carbon fiber performance. ChemSusChem *12*, 3249–3256.

Li, Q., Naik, M.T., Lin, H.-S., Hu, C., Serem, W.K., Liu, L., Karki, P., Zhou, F., and Yuan, J.S. (2018a). Tuning hydroxyl groups for quality carbon fiber of lignin. Carbon *139*, 500–511.

Li, Q., Serem, W., Dai, W., Yue, Y., Naik, M., Xie, S., Karki, P., Liu, L., Sue, H.-J., Liang, H., et al. (2017a). Molecular weight and uniformity define the mechanical performance of lignin-based carbon fiber. J. Mater. Chem. A. *5*, 12740–12746.

Li, Q., Xie, S., Serem, W.K., Naik, M.T., Liu, L., and Yuan, J.S. (2017b). Quality carbon fibers from fractionated lignin. Green. Chem. *19*, 1628–1634.

Li, X., Weng, J.-K., and Chapple, C. (2008). Improvement of biomass through lignin modification. Plant J. *54*, 569–581.

Li, Y., Shuai, L., Kim, H., Motagamwala, A.H., Mobley, J.K., Yue, F., Tobimatsu, Y., Havkin-Frenkel, D., Chen, F., Dixon, R.A., et al. (2018b). An "ideal lignin" facilitates full biomass utilization. Sci. Adv. *4*, eaau2968.

Liu, E., Li, M., Das, L., Pu, Y., Frazier, T., Zhao, B., Crocker, M., Ragauskas, A.J., and Shi, J. (2018). Understanding lignin fractionation and characterization from engineered switchgrass treated by an aqueous ionic liquid. ACS Sustain. Chem. Eng. *6*, 6612–6623.

Mainka, H., Täger, O., Körner, E., Hilfert, L., Busse, S., Edelmann, F.T., and Herrmann, A.S. (2015). Lignin – an alternative precursor for sustainable and cost-effective automotive carbon fiber. J. Mater. Res. Technol. *4*, 283–296.

Maity, S.K. (2015). Opportunities, recent trends and challenges of integrated biorefinery: Part I. Renew. Sustain. Energy Rev. *43*, 1427–1445.

Mansfield, S.D., Kang, K.-Y., and Chapple, C. (2012). Designed for deconstruction – poplar trees altered in cell wall lignification improve the efficacy of bioethanol production. New Phytol. *194*, 91–101.

Meng, X., Pu, Y., Yoo, C.G., Li, M., Bali, G., Park, D.-Y., Gjersing, E., Davis, M.F., Muchero, W., Tuskan, G.A., et al. (2017). An in-depth understanding of biomass recalcitrance using natural poplar variants as the feedstock. ChemSusChem *10*, 139–150.

Mohanty, A.K., Vivekanandhan, S., Pin, J.-M., and Misra, M. (2018). Composites from renewable and

sustainable resources: challenges and innovations. Science *362*, 536–542.

Pilate, G., Guiney, E., Holt, K., Petit-Conil, M., Lapierre, C., Leplé, J.-C., Pollet, B., Mila, I., Webster, E.A., Marstorp, H.G., et al. (2002). Field and pulping performances of transgenic trees with altered lignification. Nat. Biotechnol. *20*, 607–612.

Ragauskas, A.J., Beckham, G.T., Biddy, M.J., Chandra, R., Chen, F., Davis, M.F., Davison, B.H., Dixon, R.A., Gilna, P., and Keller, M. (2014). Lignin valorization: improving lignin processing in the biorefinery. Science *344*, 709–809.

Singer, L.S. (1981). Carbon fibres from mesophase pitch. Fuel *60*, 839–847.

Studer, M.H., Demartini, J.D., Davis, M.F., Sykes, R.W., Davison, B., Keller, M., Tuskan, G.A., and Wyman, C.E. (2011). Lignin content in natural Populus variants affects sugar release. Proc. Nat. Acad. Sci. USA *108*, 6300–6305.

Thomas, V.A., Kothari, N., Bhagia, S., Akinosho, H., Li, M., Pu, Y., Yoo, C.G., Pattathil, S., Hahn, M.G., Raguaskas, A.J., et al. (2017). Comparative evaluation of Populus variants total sugar release and structural features following pretreatment and digestion by two distinct biological systems. Biotechnol. Biofuels *10*, 292–307.

Titirici, M.M., White, R.J., Brun, N., Budarin, V.L., Su, D.S., Del Monte, F., Clark, J.H., and Maclachlan, M.J. (2015). Sustainable carbon materials. Chem. Soc. Rev. *44*, 250–290.

Tuck, C.O., Pérez, E., Horváth, I.T., Sheldon, R.A., and Poliakoff, M. (2012). Valorization of biomass: deriving more value from waste. Science *337*, 695–699.

Van Acker, R., Leplé, J.-C., Aerts, D., Storme, V., Goeminne, G., Ivens, B., Légée, F., Lapierre, C., Piens, K., Van Montagu, M.C.E., et al. (2014). Improved saccharification and ethanol yield from field-grown transgenic poplar deficient in cinnamoyl-CoA reductase. Proc. Nat. Acad. Sci. USA *111*, 845–850.

Wagner, A., Tobimatsu, Y., Phillips, L., Flint, H., Geddes, B., Lu, F., and Ralph, J. (2015). Syringyl lignin production in conifers: proof of concept in a Pine tracheary element system. Proc. Nat. Acad. Sci. USA *112*, 6218–6223.

Wang, H., Pu, Y., Ragauskas, A., and Yang, B. (2019). From lignin to valuable products–strategies, challenges, and prospects. Bioresour. Technol. *271*, 449–461.

Yoo, C.G., Dumitrache, A., Muchero, W., Natzke, J., Akinosho, H., Li, M., Sykes, R.W., Brown, S.D., Davison, B., Tuskan, G.A., et al. (2018). Significance of lignin s/g ratio in biomass recalcitrance of populus trichocarpa variants for bioethanol production. ACS Sustain. Chem. Eng. *6*, 2162–2168.

Zhang, R., Du, Q., Wang, L., Zheng, Z., Guo, L., Zhang, X., Yang, X., and Yu, H. (2019). Unlocking the response of lignin structure for improved carbon fiber production and mechanical strength. Green. Chem. *21*, 4981–4987.

Zhao, Q., Nakashima, J., Chen, F., Yin, Y., Fu, C., Yun, J., Shao, H., Wang, X., Wang, Z.-Y., and Dixon, R.A. (2013). LACCASE is necessary and nonredundant with PEROXIDASE for lignin polymerization during vascular development in Arabidopsis. Plant Cell *25*, 3976–3987.

iScience, Volume *23*

Supplemental Information

Discovering Biomass Structural Determinants Defining the Properties of Plant-Derived Renewable Carbon Fiber

Qiang Li, Cheng Hu, Mengjie Li, Phuc Truong, Mandar T. Naik, Dwarkanath Prabhu, Leo Hoffmann Jr., William L. Rooney, and Joshua S. Yuan

1. Supplemental Data Items

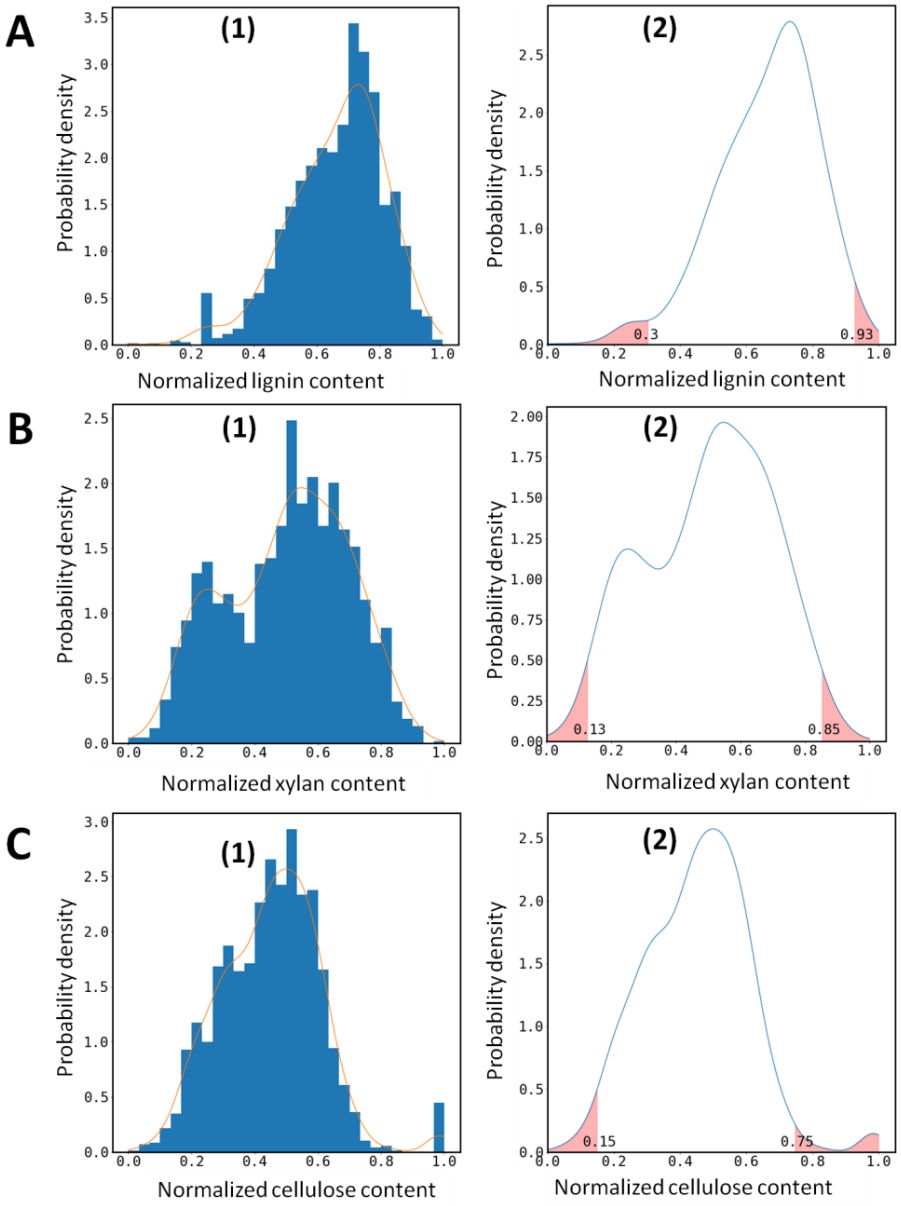

Figure S1. The histogram distributions and probability curves of each component of sorghum feedstock estimated from Kernel density, related to Figure 2a. The panel a, b, and c are lignin, xylan and cellulose, respectively. Figures in panel-1 show the histogram distribution and the figures in panel-2 show the probability density curves. The shaded pink areas are for the definition of the high and low component according to the probability density, where the lower-end 2.5% probability density was defined as the low content and the higher-end 2.5% probability density was defined as the high content.

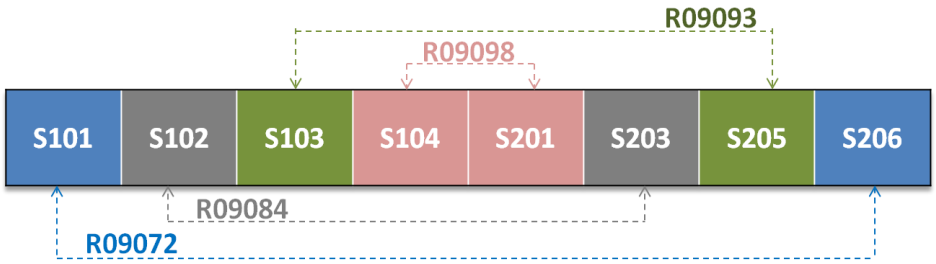

Figure S2. The field design of sorghum with four genotypes (R09072, R09084, R09098 and R09093), each of which was replicated, related to Figure 2.

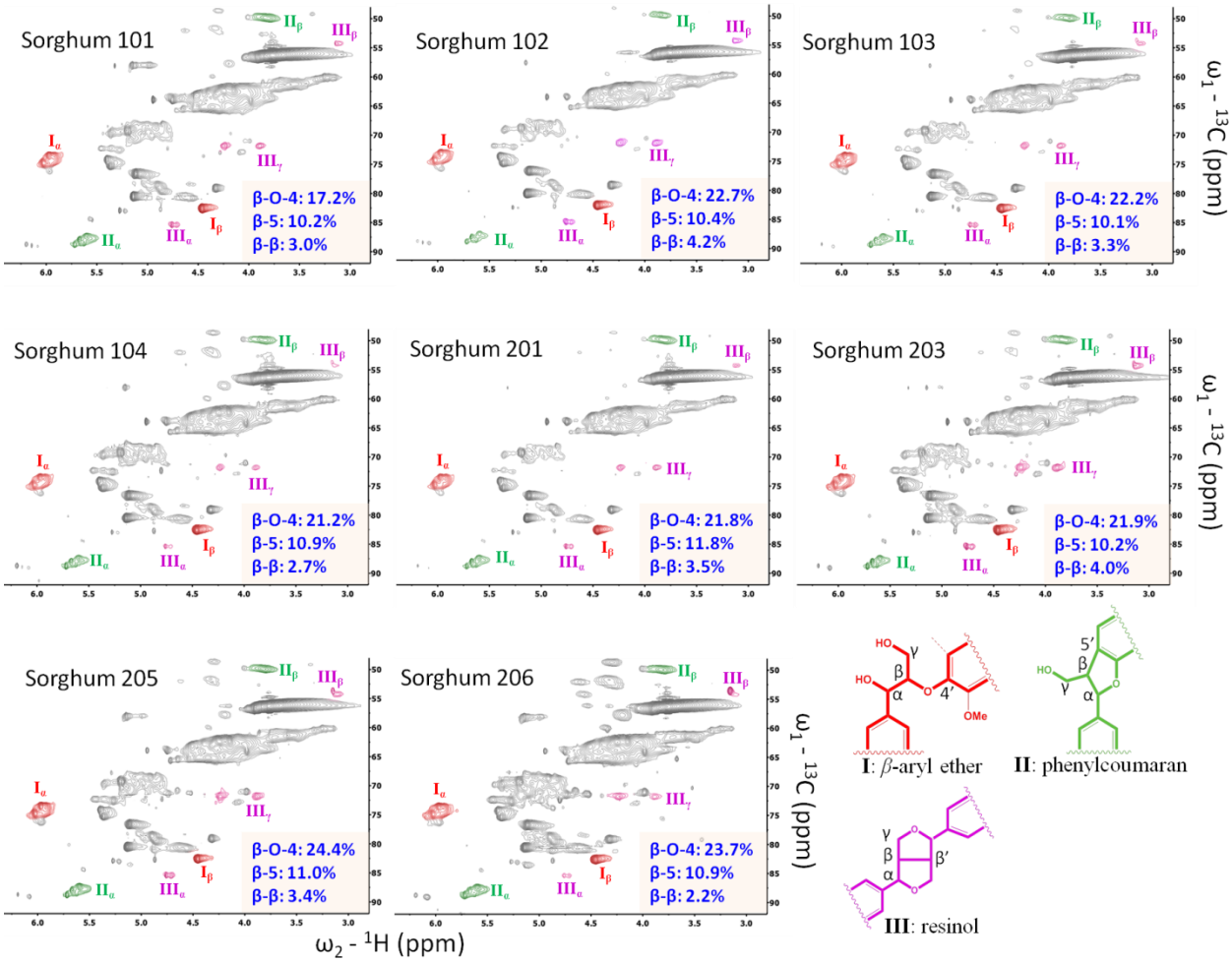

Figure S3. Internuitary linkages in the sorghum lignin as revealed by 2D HSQC NMR, related to Figure 2b3.

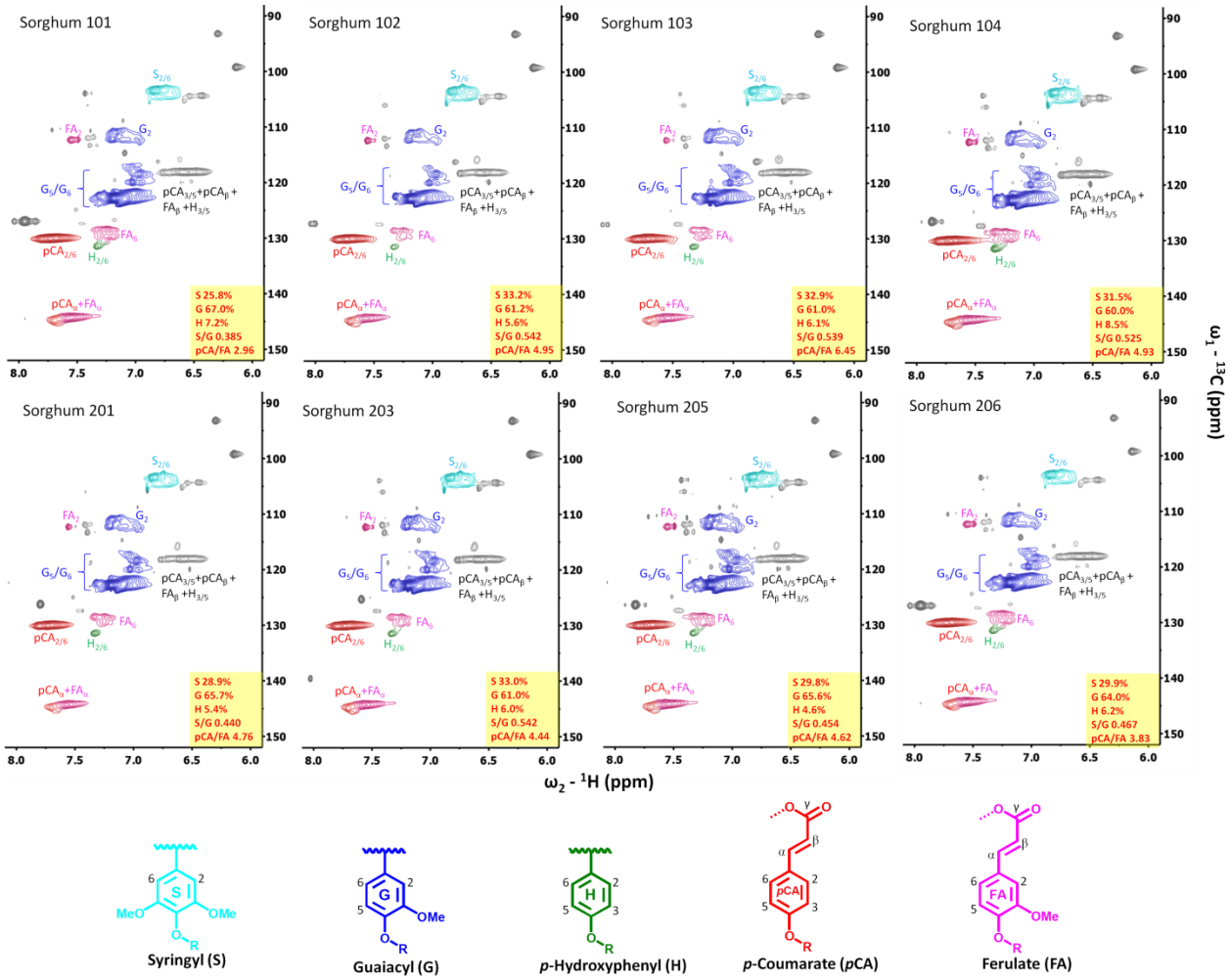

Figure S4. Aromatic regions of the 2D HSQC NMR spectra of lignin, related to Figures 2b3, 3g and 4e. G_2, G_5, and G_6 are carbon-2, carbon-5, and carbon-6 correlations from guaiacyl (G) units; $S_{2/6}$ is carbon-2 and -6 correlations from syringyl (S) units; $H_{2/6}$ is carbon-2 and -6 correlations from *p*-hydroxyphenyl (H) units; $pCA_{2/6}$ and pCA_{α} are carbon-2 and -6, and carbon-*α* correlations from *p*-coumarate (pCA) units; FA_2, FA_5, and FA_{α} are carbon-2, carbon-5, and carbon-*α* correlations from ferulate (FA) units.

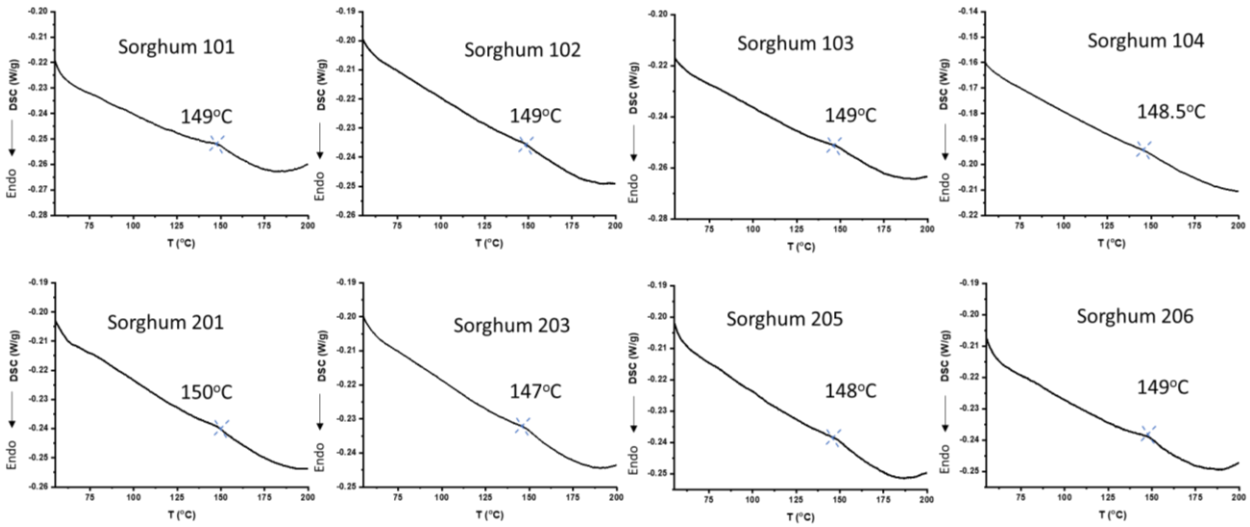

Figure S5. DSC thermograms and T_g of lignin-based as-spun fibers for sorghum variants.

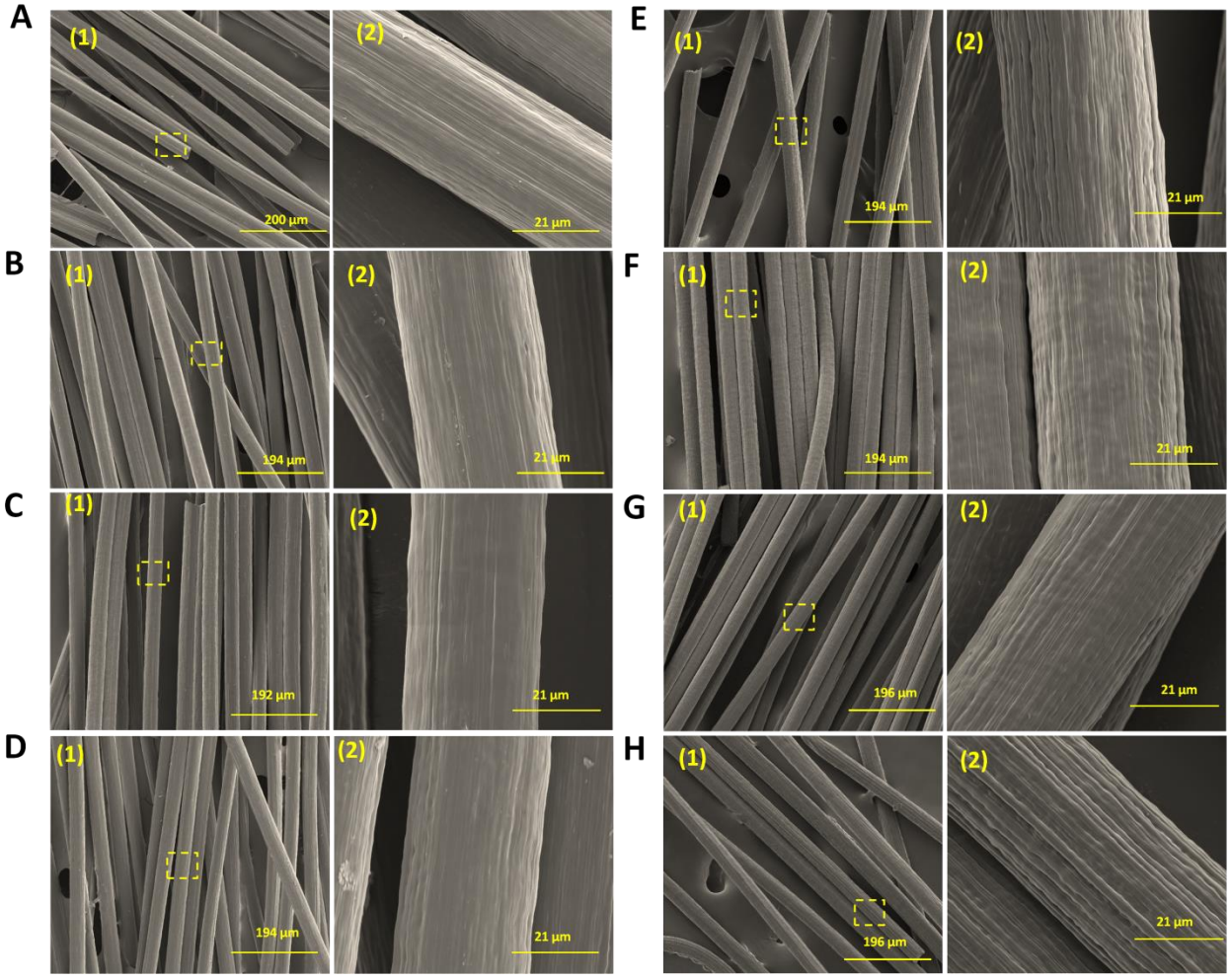

Figure S6. The morphologies of carbon fiber surfaces, related to Figure 2f. A, B, C, D, E, F, G and H are carbon fibers made of lignin from sorghum 101, 102, 103, 104, 201, 203, 205 and 206, respectively.

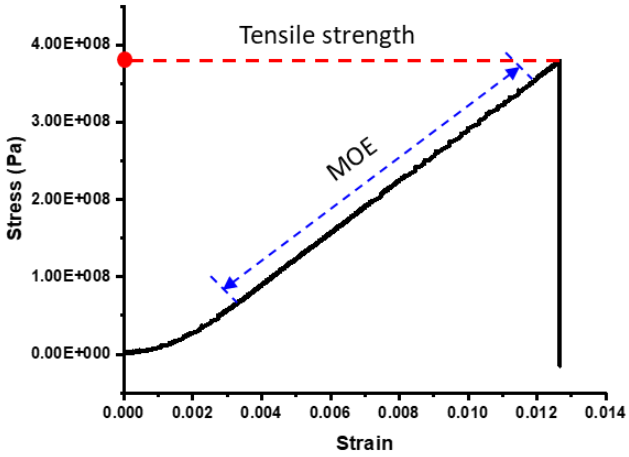

Figure S7. A typical stress-strain curve of lignin-based carbon fiber, related to Figures 3 and 4.

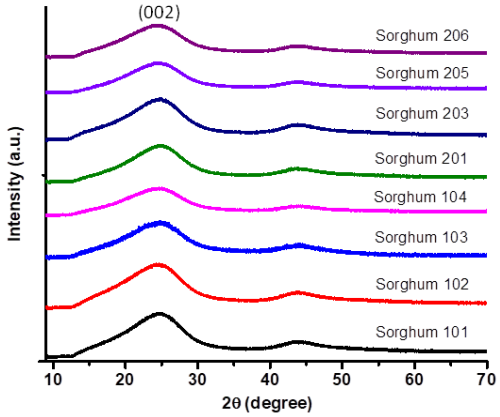

Figure S8. XRD diffractograms of carbon fibers made from sorghum lignin, related to Figures 3 and 4.

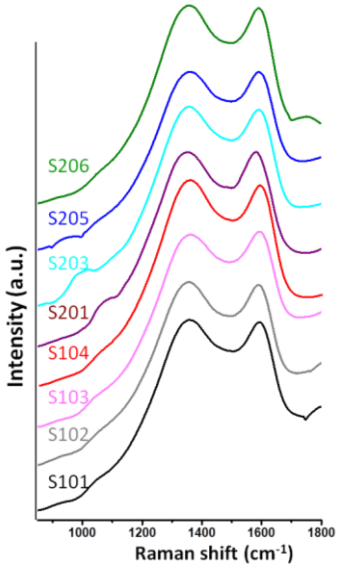

Figure S9. Raman spectra of carbon fiber made from sorghum lignin, related to Figures 3 and 4.

Table S1. Definitions of high and low components according to their component distributions, related to Figure 2a.

Sorghum	Low	Moderate	High
Lignin	< 0.30	0.30-0.90	> 0.90
Cellulose	< 0.15	0.15-0.75	> 0.75
Xylan	< 0.13	0.13-0.85	> 0.85

Table S2. Assignments of lignin chemical structures in 2D HSQC NMR, related to Figure 2b3. (Li et al., 2017b, Mansfield et al., 2012)

Lignin structures*	F2 (ppm)	F1 (ppm)
I α (α position in β–*O*–4')	6.0	74.5
IIα (α position in β–5')	5.5	87.7
IIIα (α position in β–β')	4.5	87.0
IVβ (β position in DBDO)	4.2	81.5
C_2/H_2 in guaiacyl units (G_2)	6.8	111.3
$C_{2,6}/H_{2,6}$ in ρ-hydroxyphenyl units ($H_{2/6}$)	7.3	127.2
$C_{2,6}/H_{2,6}$ in syringyl units ($S_{2/6}$)	6.7	103.8
$C_{2,6}/H_{2,6}$ in *p*-Coumarate ($pCA_{2,6}$)	7.6	130.0
C_α/H_α in *p*-Coumarate (pCA_α)	7.6	145.0
C_2/H_2 in Ferulate (FA_2)	7.5	111.5
C_6/H_6 in Ferulate (FA_6)	7.3	128.3
C_α/H_α in Ferulate (FA_α)	7.5	144.5

*Lignin linkages and units are shown in Figures S1 and S2, respectively.

Table S3. Lignin content of each sorghum sample, related to Figures 2b4, 3f and 4d.

Sorghum	Klason lignin (%)	Acid-soluble lignin (%)	Total lignin (%)
Sorghum 101	19.4	2.3	21.7
Sorghum 102	20.7	2.3	23.0
Sorghum 103	19.8	2.3	22.1
Sorghum 104	19.4	2.5	21.9
Sorghum 201	19.0	2.4	21.4
Sorghum 203	21.0	2.2	21.2
Sorghum 205	20.4	2.2	22.6
Sorghum 206	20.2	2.3	22.5

Table S4. Yields of lignin-based fibers after thermostabilization and carbonization, related to Figures 2c.

Samples	Thermostabilization (%)[a]	Carbonization (%)[b]
Sorghum 101	93.0	56.7
Sorghum 102	92.3	61.2
Sorghum 103	94.4	58.3
Sorghum 104	88.9	59.9
Sorghum 201	92.0	63.3
Sorghum 203	91.6	64.2
Sorghum 205	91.0	62.3
Sorghum 206	92.3	60.1

[a]: based on the weight of the as-spun fibers; [b]: based on the weight of thermostabilized fibers.

2. Transparent Methods

2.1 Materials

Polyacrylonitrile (PAN) used in this research was purchased from Pfaltz & Bauer, USA, and had a MW of 150,000 g/mol. All chemicals used in this research were products of Sigma–Aldrich, USA.

2.2 Selection of sorghum feedstock

Eight sorghum samples with four genotypes grown under two environments were selected from 2067 different sorghum feedstock harvested from 60 days after planting in College Station, TX.(Hoffmann and Rooney, 2014) After drying the samples, the content of lignin, hemicellulose (xylan) and cellulose were estimated using near infrared spectroscopy.(Hoffmann and Rooney, 2014) For cellulose and xylan, we have defined the highest content as

1 and the lowest one as 0 using multidimensional scaling, and thus each component has been scaled to be in the range of 0 and 1 using the formula as below:

$$\text{Scaled component content} = (C_x - C_{x\text{-min}})/(C_{x\text{-max}} - C_{x\text{-min}})$$

where C_x is the content of the component, x represents the component cellulose or xylan, $C_{x\text{-min}}$ is the minimum content of the component, and the $C_{x\text{-max}}$ is the maximum content of the component.

For lignin, the scaled content (in the range of 0 to 1) was divided by total sorghum component content to obtain a ratio of lignin to the total component and then scaled as follows:

$$C'_{lignin} = C_{lignin} / (C_{lignin} + C_{cellulose} + C_{xylan})$$

$$\text{Scaled lignin content} = (C'_{lignin} - C'_{lignin\text{-min}})/(C'_{lignin\text{-max}} - C'_{lignin\text{-min}})$$

where C_{lignin}, $C_{cellulose}$ and C_{xylan} are component contents, C'_{lignin} is the ratio of the lignin to the total component content.

The multidimensional scaling effectively built a diagram to effectively evaluate relative biomass characteristics among thousands of samples, while plotting components against each other. The scaled lignin content covers dependencies across all sorghum, and the cellulose and xylan components can be plotted against it in two dimensions. Moreover, for each scaled component, we have defined the very high and very low content according to their distributions. To calculate the distribution of each component, a histogram was plotted of available data and fit to a Kernel density estimate as shown in Figure S1, where the values were the probability density calculated using the Kernel density estimates for the data available. As shown in A1 to A3 in Figure S1, the shaded regions signify 2.5% of the area under the probability density curves on either side. The lower and higher thresholds on sorghum content were thus defined as the low component content and high component content, respectively, which were summarized as shown in Table S1.

The component distributions of all feedstock are shown in Figure 1b. Four photoperiod sorghum lines, R.09072 (sorghum 101 and 206), R.09084 (sorghum 102 and 203), R.09093 (sorghum 103 and 205) and R.09098 (sorghum 104 and 201) with duplicate for each were finally selected for this study because that they have similar cellulose and xylan distributions but very diverse lignin distribution. The field design was as shown in Figure S2.

2.3 Organosolv extraction of lignin

Lignin was extracted from sorghum using acetic acid as reported before.(Pan et al., 1998, Pan and Sano, 2005) Briefly, 90% aqueous acetic acid with 0.32% sulfuric acid as catalyst was added into 40 g of biomass. The liquid to solid ratio was 10:1. The heating temperature was kept at around 118^{o}C in an oil bath to keep acetic acid reflux. After 3-h extraction, the mixture was cool down and then filtrated to get a filtrate and biomass residue. The obtained filtrate was then concentrated into about 100 mL by evaporation, and followed by precipitation into pH 2 deionized water and stirring for 30 min. After centrifugation, three times washing with deionized water, centrifugation again, and lyophilization, fine lignin powders can be obtained.

2.4 Lignin Characterizations

2.4.1 Lignin content in sorghum

Lignin content in sorghum was measured using the classic Klason method. The experiment followed the NREL procedures with slight modifications (Sluiter et al, 2012). Briefly, 300 ± 10 mg biomass was treated with 3 mL of 72 % sulfuric acid at room temperature first. The sulfuric acid was then diluted to 4% followed by autoclaving the samples at 121 ^{o}C for 1-h. The acid insoluble part as Klason lignin was weighted after filtration and drying. The acid soluble part was measured using a UV-visible spectroscopy at 280 nm and calculated with the absorptivity of $E^{1\%}_{280nm} = 19.9$ L/g cm. Lignin content was reported as the total content of Klason lignin and the acid-soluble lignin. Each sample was measured twice to get an average result. The details of the Klason lignin and the acid-soluble lignin for each sorghum sample were in Table S2.

2.4.2 Size exclusion chromatography (SEC)

Molecular weight and polydispersity of sorghum lignin was measured by a Tosoh ECOSEC system (HLC-8320GPC, Tosoh Bioscience LLC, Grove City, OH). Before the characterization, all lignin samples were acetylated as reported.(Chen 1992) The conditions for SEC were: column, one TSKgel Super HZM-M column (4.6mm ID X 15 cm, 3&5 um) and one TSKgel Super HZM-M column (4.6mm ID X 15 cm, 4 um) were connected in series, and one TSKgel SuperH-RC column (6.00mm ID x 15cm) was used as the reference column; column temperature, 40 °C; eluent, tetrahydrofuran (THF); flow rate, 0.35 mL/min; detector, built-in differential refractometer (RI) and TOSOH UV Detector (UV-8320, 254 nm); injection volume, 10 μL; sample concentration, 1 mg/mL. Polystyrenes with molecular weight (Mp) of 472, 1920, 3250, 10250, 24000, 32500, and 67522 g/mol were used as standards.

2.4.3 2D Heteronuclear Single Quantum Coherence (HSQC) NMR

Lignin composition (S/G ratio) and interunitary linkages were characterized with 2D HSQC NMR. Lignin (30-50 mg) was dissolved in 0.6 mL of DMSO-*d6* and placed in a NMR tube. Adiabatic 2D ^{1}H-^{13}C HSQC spectra were acquired using a Bruker Avance-III 400 MHz spectrometer equipped with a 5 mm Broadband Observe probe (5 mm BBO 400 MHz W1 with Z-gradient probe, Bruker) and a Bruker standard pulse sequence ('hsqcetgpsi2'). The spectra were obtained with a spectral width of 11 ppm in F2 (^{1}H, 2048 data points) and 190 ppm in F1 (^{13}C, 256 data points). 64 scans with a 1-s delay were used for each sample. The obtained HSQC spectra were then analyzed and re-processed by using software MestReNova. The assignments and quantification of linkages and S, G, H units were shown in Table S3. The semi-quantification of each interunitary linkage (Figure S3) was measured as the percentage of the volume integration of the linkage to that of the aromatic rings. The volume integration of all aromatic peaks were calculated from $S_{2/6}$, G_2, and $H_{2/6}$ at δC/δH 103.8/6.70 ppm, δC/δH 113.3/6.83 ppm, and δC/δH 127.2/7.31 ppm, respectively (Figure S4), and both S and H integrals were logically halved.(Mansfield et al 2012) The results of linkage frequencies were expressed as the percentages of 100 aromatic rings. For S/G ratios calculation, the volume integration of peaks $S_{2/6}$ was divided by that of the G_2. S integrals were logically halved as above before the calculation.

2.4.4 Differential Scanning Calorimetry (DSC)

As we reported before,(Li et al, 2017b) DSC was conducted using a TA Q2500 system (TA Instruments, New Castle, DE) under N_2 atmosphere. Five milligram of lignin samples were placed in a sample pan and then heated from 0 °C to 400 °C with two cycles at the heating and cooling rates of 10 °C/min. The glass transition temperature (T_g) was derived from the second cycle of DSC analysis. All DSC thermograms and the measured T_g were in Figure S5. We did not observe significant difference in the T_g between lignin from different sorghum variants, indicated that lignin uniformity may not impact the glass transition temperature of lignin from sorghum variants. Moreover, these lignin samples might have similar miscibility with guest PAN polymers.

2.5 Carbon fiber preparation

2.5.1 Wet spinning

Lignin was spun into fibers by a customized wet spinning unit as reported before.(Li et al. 2019b) Briefly, lignin/PAN dopes were prepared with a weight ratio of 50/50 and a concentration of 10% in DMF. The dopes were sonicated for 30 minutes to remove possible air bubbles before spinning. To form fibers, wet spinning was carried out by injecting the spinning dopes into a methanol coagulation bath (-20 °C) at a rate of 0.08 mL/min. As-spun fibers were winded on a rolling drum. After washing with deionized water, the fibers were cut and hanged under 15 g load until dry.

2.5.2 Thermostabilization

As-spun fibers were thermostabilized under atmosphere using a muffle furnace (GSL 1200X, MTI Corporation, Richmond, CA). The fibers were placed in crucibles and heated from room temperature to 250 °C with a heating rate of 1 °C/min. The holding time at 250 °C was 1 h, which was followed by automatically cooling down.

The yields of the thermostabilized fibers were calculated based on the weights of the as-spun fibers that have been used for thermostabilization. As shown in Table S4, the highest yield was 94.4 % for Sorghum 103, while the lowest one was 88.9% for Sorghum 104. Nevertheless, no significant difference of the yields was observed between other sorghum variants.

2.5.3 Carbonization

Carbonization of thermostabilized fibers was carried out in a split tube furnace with vacuum system (GSL 1600X, MTI Corporation, Richmond, CA) under argon atmosphere (240 cm^3/min). The temperature for carbonization was increased from room temperature to 1 000 °C with a heating rate of 5 °C/min. The holding time at 1000 °C was 1 h.

The calculation of the yields of the carbonized fibers were based on the weights of the thermostabilized fibers that have been used for carbonization. As shown in Table S4, the yield ranged from 56.7% for Sorghum 101 to 64.2% for Sorghum 203.

2.6 Carbon fiber characterizations

2.6.1 Field emission scanning electron microscope (FE-SEM)

Carbon fibers were coated with 10 nm iridium (Ir) and then observed under a Quanta 600F FE-SEM (FEI Company, Hillsboro, OR). The working distance was 10 mm, and the accelerating voltage applied was 5 kV. To get the morphologies of carbon fiber cross sections, fibers were mounted vertically on the SEM sample holder and then observed using the FE-SEM under the same conditions. The morphologies of carbon fiber surfaces were shown in Figure S5 and the morphologies of carbon fiber cross sections were displayed in Figure 2f.

2.6.2 Tensile test

The mechanical properties of carbon fibers were measured under a TestResources universal mechanical tester (Shakopee, MN) as reported before.(Li et al. 2019b) Briefly, fibers were mounted on a sample holder made of paper board, which was then fixed on two grippers. For the measurement, a 2 N load cell with the resolution of 0.0001 N was used and the displacement rate was set at 0.200 mm/min. The original length (L) of fibers was measured by using a vernier caliper, and the area (A) of each fiber was measured under aforementioned FE-SEM after the test. Stress-strain curves (Figure S7) can be plotted after getting stress (σ) and strain (ε) using the equations of $\sigma = F/A$ and $\varepsilon = d/L$, respectively, where F is the applied force and d is the corresponding displacement. As shown in Figure S7, the tensile strength was calculated from the maximum stress at fracture in the stress-strain curve, while the modulus of elasticity (MOE) was calculated from the slop of the elastic deformation region, respectively. Elongation (%) was calculated by $d'/L \times 100$, where d' is the displacement at the fracture. For each sample, at least 15 different fibers were measured to get an average data.

2.6.3 X-ray diffraction (XRD)

XRD analysis of carbon fiber crystallite structure was performed under a Bruker D8 Discovery XRD (Bruker, Madison, WI). To avoid the orientation preference, carbon fibers were ground into fine powders by an agate mortar and pestle before the measurement. X-ray resource was generated at 40 kV voltage and 40 mA current with Cu Ka wavelength (λ) of 1.542 Å. Scanning range (2θ) was from 8° to 55°, scanning step size was 0.05°, and scanning rate was set at 1.5°/min. The XRD diffractograms of lignin-based carbon fibers were shown in Figure S6. The crystalline size (L_{hkl}) was calculated from (002) panel around 2θ of 24.5° by using Scherrer equation: $L = \frac{K\lambda}{\beta \cos\theta}$, where L is the crystalline size, nm; K is shape factor, set as 0.94 in this calculation; λ is the X-ray wavelength (1.542 Å); β is the full width at half maximum (FWHM) in radian; θ is the Bragg angle in degree. The distance between two crystalline lattices (d_{hkl}) was estimated by using Bragg's law: $2d \sin\theta = n\lambda$, where d is distance in nm; θ is the Bragg angle in degree; n is set as 1.

2.6.4 Raman Spectroscopy

The ground carbon fiber powder was mounted on a glass slide with the help of a double adhesive tape, and Raman spectra were taken under a Horiba Jobin-Yvon LabRam Raman Confocal Microscope with 633 nm laser, 10× magnification of objective lens, D0.3 filter, 200 μm confocal pinhole, 10 s exposure time, and 10 accumulations. The Raman spectra of lignin carbon fibers were shown in Figure S7. D band (1348 cm^{-1}) and G band (1581 cm^{-1}) were deconvoluted by Guassian curve fitting method using Origin 9 software. The G/D ratios were calculated from the area ratios of these two bands.

3. Supplemental Reference

C-L, Chen. (1992). Determination of total and aliphatic hydroxyl groups. *In: Methods in lignin chemistry* Lin, S. Y., Dence, C. W (ed.). NY: Springer–Verlag.

Mansfield, S. D., Kim, H., Lu, F. and Ralph, J. (2012). Whole plant cell wall characterization using solution-state 2D NMR. Nat. Protocols *7*, 1579-1589.

Pan, X.-J., Sano, Y., Nakashima, H. and Uraki, Y. (1998). Atmospheric acetic acid pulping of rice straw (1) pulping conditions and properties of pulp. Japan TAPPI J. *52*, 408-415.

PAN, X. and SANO, Y. (2005). Fractionation of wheat straw by atmospheric acetic acid process. Bioresource Technol. *96*, 1256-1263.

Sluiter, A., Hames, B., Ruiz, R., Scarlata, C., Sluiter, J., Templeton, D. & Crocker D. (2012). Determination of structural carbohydrates and lignin in biomass. NREL laboratory analytical procedure (LAP).